A Close-Up Investigation of Halftone Color Prints

Daniel Nyström*

Keywords: Color print reproduction, Optical dot gain

Abstract: Modeling the color reproduction of halftone prints is difficult, because of light scattering, causing optical dot gain. Most available models are limited to macroscopic color measurements, averaging the reflectance over an area that is large relative the dot size. The aim of this study is to go beyond the macroscopic approach and study optical dot gain on a micro-scale level, using colorimetric images of printed halftones. An experimental imaging system, combining the accuracy of color measurement instruments with a high spatial resolution, opens up possibilities to better study the color reproduction in halftone color prints. The main focus is to study how the reflectance values of the printed dots and the paper between the dots, $R_i(F_i)$ and $R_p(F_i)$, vary with the dot area fraction.

Micro-scale images, i.e. when the resolution of the images is high in relation to the resolution of the halftone, allow for measurements of the individual halftone dots, as well as the paper between them. To capture the characteristics of large populations of halftone dots, histograms are computed. From the histogram data it is possible to derive the mean reflectance, R, the reflectance for the dots, $R_i(F_i)$, and the paper between the dots, $R_p(F_i)$. The true dot area coverage, including the physical dot gain, is computed using histogram data, as well as using line scans in the micro-scale images.

A previously proposed extension of the Murray-Davies equation, incorporating $R_i(F_i)$ and $R_p(F_i)$, is evaluated. The model is further extended to handle color prints, predicting tristimulus values, by using 3D histograms in CIEXYZ color space. To reduce the complexity, projection from XYZ coordinates into one-dimensional color distributions are used. The prediction errors of the model were found to be equivalent, or better, to that of the Yule-Nielsen model using an optimal n-factor. However, unlike Yule-Nielsen, the extended Murray-Davies model preserves the linear additivity of reflectance, thus providing a better physical description of optical dot gain in halftone color prints.

*Linköping University, Dept of Science and Technology (ITN)
SE-60174 Norrköping, Sweden

Introduction

Over the years, many models have been proposed to predict the outcome of halftone prints. The task is difficult, partly because of light scattering within the halftone image, causing optical dot gain, also known as the Yule-Nielsen effect. On the other hand, optical dot gain often co-exists with the so called physical dot gain, caused by physical dot extension in the printing process. Understanding the physical nature and accurate models of optical dot gain in halftone prints are essential for accounting for the effect in order to improve print quality.

In the 1930s Murray and Davies published the first model to predict the output reflectance of a halftone print (Murray, 1936). The mean reflectance R, is simply given by linear interpolation of the reflectance of the bare paper, R_p, and the full tone, R_i, weighted by the dot area fraction, F_i, as:

$$R(F_i) = F_i R_i + (1 - F_i) R_p \tag{1}$$

The famous Neugebauer model is then a relatively straightforward extension of Murray-Davies, to handle the multiple colorants in color printing. Since the reflected light from different areas is added to predict the overall reflectance, these models preserve the linearity of photon additivity. It is, however, well known that the performance of these linear models is very limited. The relationship of R versus F_i is in fact non-linear, due to light scattering in the paper substrate, causing optical dot gain.

In the 1950s, Yule and Nielsen published their famous work on light penetration and scattering in paper (Yule & Nielsen, 1951). It was then shown that the nonlinear relationship could be approximated by a power function, as:

$$R(F_i) = \left[F_i R_i^{1/n} + (1 - F_i) R_p^{1/n} \right]^n \tag{2}$$

The Yule-Nielsen (Y-N) *n-factor*, accounting for light scattering in the paper, is an empirically derived constant, selected to provide the best fit to experimental data. Unless other factors than optical scattering of light are involved, values of n between 1 and 2 are physically meaningful, with n =2 corresponding to a highly scattering substrate. It has been suggested that an average n value of 1.7, should be satisfactory when the real value is unknown (Pearson, 1980). However, with modern high-resolution printers, values of n greater than 2 are often required (Wyble & Berns, 2000). The Y-N model is still commonly used, because it works relatively well. However, it does not physically describe or explain the phenomenon of optical dot gain, and the conservation of energy is lost when the nonlinear transform is applied to the reflectance values. Notice

that the fundamental assumption in these models is that the color for the substrate and the ink is both uniform and constant, which is rarely the case in reality.

In the 1990s, it was showed that the color of the halftone dots and the paper between the dots is not constant, but dependent on the dot area fraction, F_i (Engeldrum, 1994). The reflectance of the printed halftone dots, as well as the paper between them, decreases with increased dot area coverage, due to the light scattering in the substrate. En expanded Murray-Davies model was later proposed, with the constants for paper and ink reflection replaced by the functions $R_i(F_i)$ and $R_p(F_i)$ (Arney, et al., 1995a, 1995b):

$$R(F_i) = F_i R_i(F_i) + (1 - F_i) R_p(F_i) \tag{3}$$

This model preserves the linear additivity of reflectance while the non-linear relation between R and F_i caused by optical dot gain, is now accounted for by using the functions $R_i(F_i)$ and $R_p(F_i)$. Naturally, the difficulty with this approach is to derive $R_i(F_i)$ and $R_p(F_i)$, i.e. the way that the "colors" of the ink and paper shift with varying dot area fraction. It is clear that it is not possible to derive these components using macroscopic measurements, giving only averaged reflectance of the print. Clearly there is a need for accurate color measurements also on a micro-scale level.

Previous attempts to measure and characterize $R_i(F_i)$ and $R_p(F_i)$ have been made by point wise measurements using a spectroradiometer equipped with magnification lenses (Engeldrum, 1994). Spectral and colorimetric values for the halftone dots and the paper between the dots were measured, using a field of view corresponding to a circle of 0.13 mm in diameter. Clearly, the method is not sufficient to derive measurements on a micro-scale level, for today's high resolution prints. Furthermore, the limited number of measurements will not necessarily be representative for a large population of halftone dots. Later on, histogram data from grayscale images have been used to compute the micro-reflectance values for the dots and the paper (Arney, et al., 1995a). The results were promising, but the application was limited to monochrome grayscale prints, and the maximal print resolution was only 330 dpi.

In this work, we continue the approach of micro-scale measurements of the reflectance of halftone dots and the paper between them. An experimental imaging system, combining the accuracy of color measurement instruments with a high spatial resolution, is used to capture micro-scale images of halftone prints. The aim is to investigate if histogram data from such images can be used to measure and characterize $R_i(F_i)$ and $R_p(F_i)$, for both grayscale and color prints. The validity of Eq. 3 is evaluated also for today's high resolution prints, and an extension to tristimulus values is proposed, using 3D histograms in

CIEXYZ color space. Different methods to compute the true dot area, F_i, a task that involves determining the physical dot gain, are described and evaluated.

Methods

The possibility to acquire colorimetric and multispectral images of prints opens up possibilities to properly characterize the microstructure of color halftones. Micro-scale images, i.e. when the resolution of the images is high in relation to the resolution of the halftone, allow for measurements of the individual halftone dots, as well as the paper between them. The details of the image acquisition system, the printed halftone samples and the experimental setup are given in the appendix.

Reflectance histograms

To capture the typical characteristics of a large population of halftone dots, which may differ in their appearance, histograms are computed from the micro-scale images. A histogram is merely a probability density function for the occurrence of different colors or reflectance values in the image, and contains nominally no spatial information. However, with the a priori knowledge that the image represents a halftone print captured in micro-scale, one can relate properties of the histogram to spatial properties of the halftone, such as the edges of the halftone dots (Arney & Wong, 1998, Nyström & Kruse, 2005).

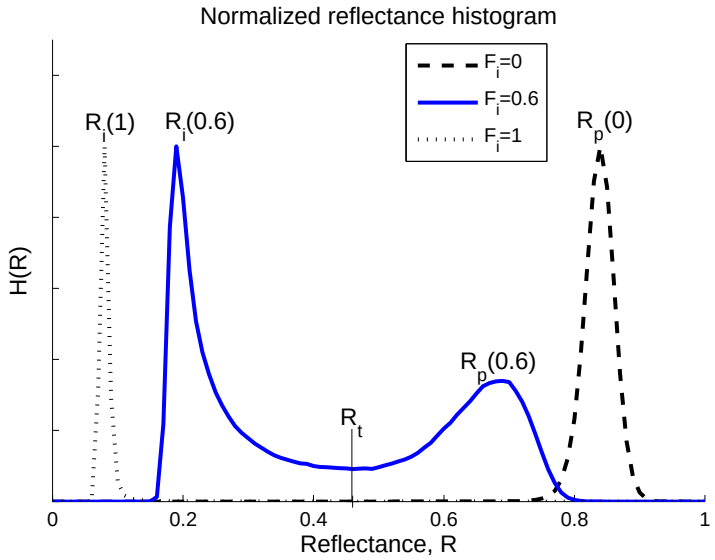

Figure 1. Normalized reflectance histogram for grayscale halftone prints of F_i=0, F_i=0.6 and F_i=1.

Figure 1 displays an example of a normalized histogram of reflectance values, for the full tone $F_i = 1$; the bare paper, $F_i = 0$; and a 60% tint. The histogram is a plot of the frequency of occurrence of the reflectance values in the images, as a function of the reflectance, R. For a perfectly reproduced halftone pattern, the histogram would be truly bimodal. For a real print, however, the populations around R_i and R_p are typically spread out, due to the spread or blurring of the halftone dots. In the histogram, the two peaks of the solid line curve correspond to the ink dots and the paper between the dots. The valley between the peaks corresponds to the edges of the halftone dots. It is clear from the positions of the peaks, for the 60% tint, that the reflectance values of the ink, $R_i(0.6)$, and paper, $R_p(0.6)$, have shifted with the dot area coverage, F_i.

From the histogram data it is possible to derive the mean reflectance of the print, R, as well as the micro reflectance for the dots, $R_i(F_i)$, and that of the paper between the dots, $R_p(F_i)$. The mean reflectance, R, corresponding to the macroscopic measurement, is given by integral:

$$R = \int_0^1 R \cdot H(R) dr \tag{4}$$

The integral can be divided into two parts, corresponding to the contribution from the ink and from the paper, respectively:

$$R = \int_0^{R_t} R \cdot H(R) dr + \int_{R_t}^1 R \cdot H(R) dr \tag{5}$$

where R_t is a reflection threshold value, defining the transition between the printed dot and the paper. If the reflection of the ink and the paper is approximated by the peak values from the histogram, $R_i(F_i)$ and $R_p(F_i)$, then Eq. 5 becomes:

$$R = R_i(F_i) \int_0^{R_t} H(R) dr + R_p(F_i) \int_{R_t}^1 H(R) dr \tag{6}$$

The integrals in Eq. 6 correspond to the area fractions for the ink, F_i, and the paper, $F_p = (1\text{-}F_i)$, and Eq. 6 thus reduces to the expanded Murray Davies according to Eq. 3. (Arney, et al., 1995a)

Finding the true dot area fraction, F_i

It is important that the dot area fraction, F_i, used in Eq. 3 corresponds to the true dot area fraction, which may differ from the commanded F_i, due to physical dot gain in the printing process. The true dot area fraction can be computed from the histogram, using a threshold value, R_t, as the limit between the ink and the paper, as:

$$F_i = \frac{\int_0^{R_t} H(R)dr}{\int_0^1 H(R)dr} \tag{7}$$

The most straight forward approach to define the threshold, R_t is to use the midpoint between the peaks corresponding to $R_i(F_i)$, and $R_p(F_i)$ in the histogram. Because no extra data are needed beside $R_i(F_i)$ and $R_p(F_i)$, this approach can also be used in cases when only these components are available.

When micro-scale images of the prints are available, another possibility is to derive the threshold from image data. By using vertical and horizontal line scans across the halftone dots, R_t can be defined as the region of maximum rate of change in reflectance values, dR/dx (Arney, et al., 1995a). An edge is a part of the image where the tone variation is large, and R_t, representing the boundary between the dot and the paper, is thus defined as the steepest slope in reflection between dot and paper. To ensure that the threshold value is representative for all halftone dots, every tenth line in the image, both horizontally and vertically, are used when computing R_t. Figure 2 illustrates an example of a scan line through a few halftone dots, along with the corresponding value of R_t and the points of maximum rate of change, dR/dx, for each edge between ink and paper.

With the possibility to capture transmission images of the same halftone patches, using a look through illumination, another possibility to compute the true dot area coverage, F_i, is available. The transmission images capture the halftone without the effect of optical dot gain, since there is no reflected light that has been scattered within the substrate. The mean intensity for each patch, I, and the intensity for the bare paper and full tone ink, I_p and I_p, are computed from the transmission images. Then the true dot area fraction is given by (compare to Eq. 1):

$$F_i = \frac{I - I_i}{I_p - I_i} \tag{8}$$

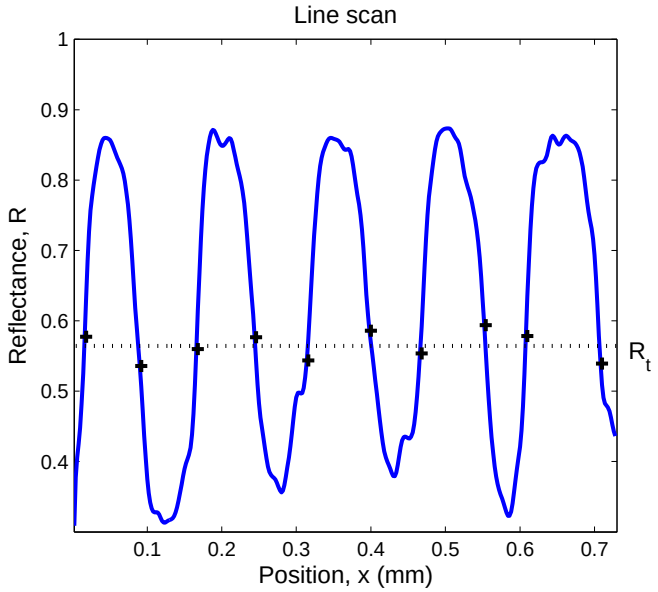

Figure 2. Illustration of a line scan (solid) across halftone dots, with the maximum rate of change dR/dx (+) and the resulting threshold value, R_t (dotted).

Color prints

When extending the method to handle color printing, the reflectance values in Eq. 3 are replaced by the CIEXYZ tristimulus values for the ink and the paper, $XYZ_p(F_i)$ and $XYZ_i(F_i)$. After converting the images into CIEXYZ color space (see the appendix), 3D color histograms are computed. In the 3D histograms, the paper and the inks appear as clusters, with the transitions between the clusters corresponding to the edges of halftone dots. The tristimulus values of the paper and the ink, $XYZ_p(F_i)$ and $XYZ_i(F_i)$, can then be computed as the centers of gravity of the clusters corresponding to the paper and ink, for each area coverage, F_i. The threshold value R_t, is now replaced by a threshold plane in XYZ color space, located at the midpoint, orthogonal to the vector between the clusters.

However, computing full 3D histograms and performing all computations in 3D, is computationally heavy. Furthermore, for some prints the clusters are not easily defined, leading to errors in the estimations of the values for $XYZ_p(F_i)$ and $XYZ_i(F_i)$, as well as the threshold plane. Since the transitions occurring between the clusters are found to be close to one-dimensional, we suggest a projection down to one-dimensional color distributions (Nyström & Kruse, 2005). The centers of gravity for the clusters of full-tone ink and bare paper are used to create a projection-vector between the clusters. Then, an orthogonal projection of all color coordinates in the XYZ images are made onto the vector. The

resulting 1D color distributions are normalized so that 0 and 1 correspond to the centers of gravity for the unprinted paper and the full ink coverage, respectively. Figure 3 illustrates an example of projections to one-dimensional color distributions, for magenta halftones of various ink coverage, F_i.

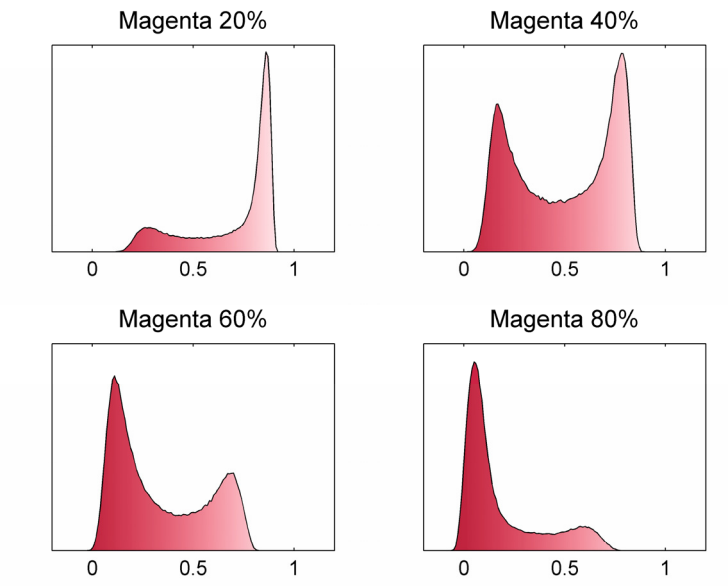

Figure 3. One-dimensional color distributions for magenta halftones, projected from CIEXYZ color space.

After computing the one-dimensional color distributions, CD, the same methodology as described for the reflectance case can be applied to find the peaks for the ink and paper in terms of the 1D color distribution, $CD_p(F_i)$ and $CD_i(F_i)$, and to compute the true dot area fraction, F_i. The resulting color values are then simply converted back to CIEXYZ tristimulus values, by using the known vector of projection.

Experimental Results

Reflectance values

Table 1 lists the RMS errors between the measured mean reflectance and the predicted reflectance values, for all printed halftone patches. The expanded Murray-Davies model (Eq. 3) has been used with $R_p(F_i)$ and $R_i(F_i)$ computed from grayscale histograms. The true dot area coverage, F_i, has been estimated using the midpoint between $R_p(F_i)$ and $R_i(F_i)$ (Mid), using line scans from micro-scale images (Line) and by using transmission images of the prints

(Trans). Computations with the Murray-Davies (MD) model and the Yule-Nielsen (YN) model are also included for comparison. For Yule-Nielsen, the optimal n-value has been used, computed individually for each print. The best results are marked as bold in the table.

Table 1. RMS errors between measured and predicted mean reflectance values.

		MD	YN	Expanded MD		
				Mid	Line	Trans
Paper A	**AM**	0.0685	0.0095	0.0084	**0.0052**	0.0539
	FM	0.1066	0.0135	0.0113	**0.0100**	0.0380
Paper B	**AM**	0.0636	0.0103	0.0065	**0.0034**	0.0144
	FM	0.0942	0.0183	0.0116	0.0136	**0.0092**
Paper C	**AM**	0.0619	0.0094	0.0098	**0.0088**	0.0145
	FM	0.1081	**0.0128**	0.0154	0.0170	0.0216
Paper D	**AM**	0.0805	0.0098	0.0093	**0.0073**	0.0254
	FM	0.1323	0.0174	**0.0116**	0.0190	0.0148
Paper E	**AM**	0.0769	0.0177	0.0100	**0.0081**	0.0207
	FM	0.0981	**0.0196**	0.0246	0.0297	0.0280

The results by employing the expanded Murray-Davies model are equivalent, or better, than the Yule-Nielsen results using optimal n-value. As expedited, the expanded Murray-Davis clearly outperforms the results for the ordinary Murray-Davis. The line scan method generally gives the best results among the different approaches to compute the true dot area fraction, F_i. The simple approach of defining the threshold as the midpoint of $R_p(F_i)$ and $R_i(F_i)$ performs surprisingly well, and generally gives better results than using transmission images. Computing the true dot area fraction from transmission images should in theory work well, but the method suffers from some practical difficulties. In the transmission images, the paper fibers become clearly visible and strongly affect the computed intensity values. The result is that the method becomes unstable, with results that depends strongly on the local structure of fibers captured in the images, which varies over the paper area.

Figure 4 displays the measured reflectance values compared to the predicted reflectance using the model, and the reflection for the ink, $R_p(F_i)$, and the paper, $R_i(F_i)$, estimated from the histograms. Clearly, the largest variation for both $R_p(F_i)$ and $R_i(F_i)$ occurs for the FM halftones, giving the strongest optical dot gain. The variation of the reflectance of the paper, $R_p(F_i)$ is generally larger than that of the ink $R_i(F_i)$. To study and model the asymptotic behaviors of $R_p(F_i)$ and $R_i(F_i)$ when F_i approaches 0 and unity, test prints containing more intermediate levels of F_i, close to 0 and 1 are needed.

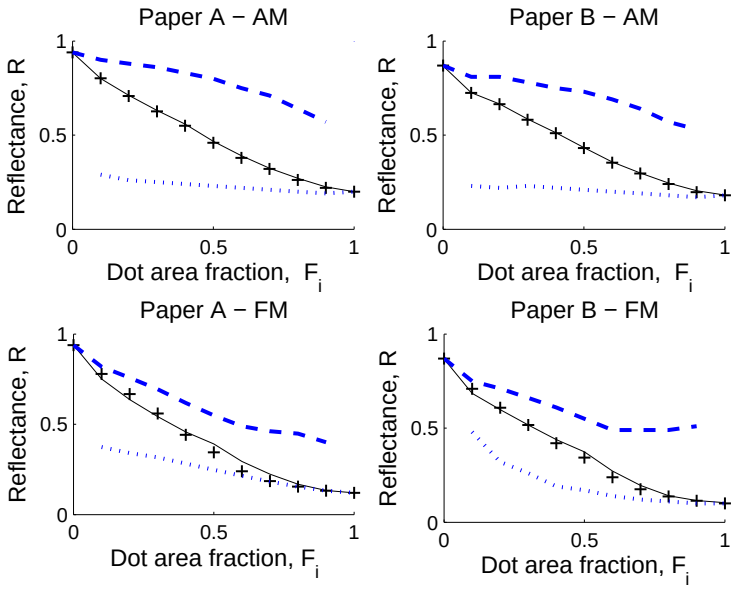

Figure 4. Measured mean reflectance (solid), predicted reflectance (+), $R_p(F_i)$ (dashed) and $R_i(F_i)$ (dotted).

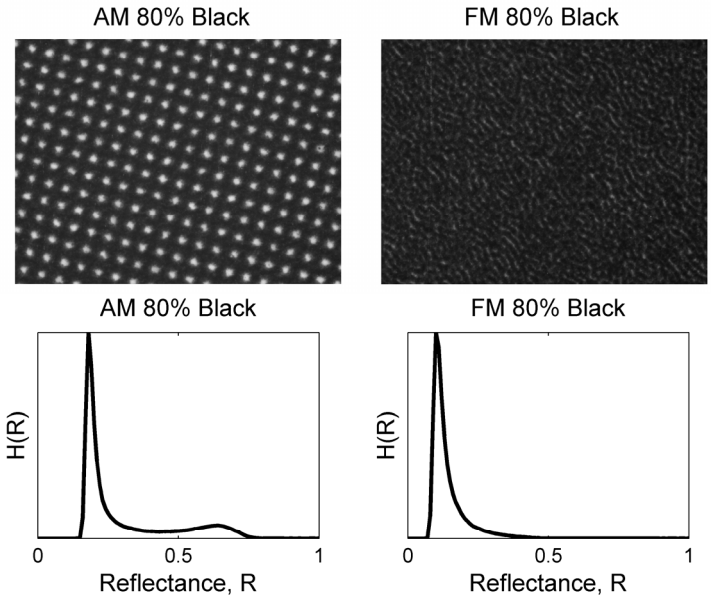

Figure 5. Images and reflectance histograms for 80% nominal ink area coverage, using AM and FM halftoning techniques.

The largest errors when applying the model clearly occur for the prints with FM halftones (Tab.1, Fig. 4). The reason is that with the small halftone dots used in the FM halftones, there is difficult to distinguish the paper from the closely spaced dots when ink coverage is high. The combination of physical and optical dot gain in the prints result in images where the paper between the dots is no longer visible. The result is that the bimodal properties of the histogram is lost, making it difficult to find the proper values of $R_p(F_i)$, and R_t, using histogram data. This is illustrated in Fig. 4d (Paper B, FM), where it is obvious that the paper reflectance, $R_p(F_i)$ has been overestimated for the higher dot area coverage, F_i. As an example, images of 80% black tints using AM and FM halftoning for the same paper grade (Paper D) are displayed in Fig. 5, along with the corresponding histograms. Clearly, the FM halftone appears more like a homogeneous gray even in micro-scale, as also suggested by its histogram where there is no peak corresponding to the reflectance of the paper.

Tristimulus values

Table 2 lists the results when the model is used to predict tristimulus values, based on the one-dimensional color distributions projected from CIEXYZ color space. The tristimulus values for the ink and paper are computed from the one-dimensional color distributions and the midpoint as used to define the threshold. The results are evaluated using the Euclidian distance in CIEXYZ color space, ΔXYZ, as well as the CIE 1976 color difference ΔE_{ab}, between the measured and predicted colorimetric values. Again, the largest estimation errors occur for the prints using the FM halftone, where the correct values for $XYZ_i(F_i)$ and $XYZ_p(F_i)$ are difficult to derive from histogram data. Generally, the black prints give the smallest estimation errors, and the largest errors appear for the yellow prints. The reason is that the tristimulus values for the yellow ink are much closer to those for the paper, making it harder to clearly separate the ink from the paper in histogram.

Figure 6 illustrates how the CIE chromaticity coordinates, x=X/(X+Y+Z) and y=Y/(X+Y+Z), varies with the dot area coverage, for the paper and the ink. The central points correspond to the chromaticity for the paper and the cluster of points at the extremes to the ink chromaticity for the primary colors cyan, magenta and yellow. It is noticeable that the chromaticity varies along straight lines, both for the ink and the paper.

Figure 7 displays the measured and predicted tristimulus values for the black print (Paper A, AM), as well as how the tristimulus values for the ink and the paper, $XYZ_i(F_i)$ and $XYZ_p(F_i)$, varies with the dot area coverage, F_i. The measured and predicted tristimulus values for Paper A using FM halftoning are displayed in Fig. 8, for the cyan, magenta, yellow and black colors.

Table 2. Estimation errors between measured and predicted tristimulus values.

		ΔXYZ max	**ΔXYZ mean**	**ΔE_{ab} max**	**ΔE_{ab} mean**
Paper A AM	Black	3.37	1.34	3.47	1.78
	Cyan	2.22	1.09	3.46	1.87
	Magenta	4.31	2.51	6.67	4.35
	Yellow	4.50	1.89	4.85	2.07
Paper A FM	Black	3.07	1.21	6.03	3.21
	Cyan	8.80	2.97	8.00	4.20
	Magenta	5.14	3.54	10.85	7.07
	Yellow	3.59	2.25	10.76	3.44
Paper D AM	Black	2.40	0.99	2.51	1.31
	Cyan	5.71	3.46	7.54	4.67
	Magenta	3.43	2.07	7.58	4.46
	Yellow	6.57	3.67	11.53	4.92
Paper D FM	Black	2.50	0.99	5.71	2.70
	Cyan	10.02	4.38	12.63	6.51
	Magenta	12.35	3.97	14.71	6.57
	Yellow	17.85	4.11	14.92	4.68

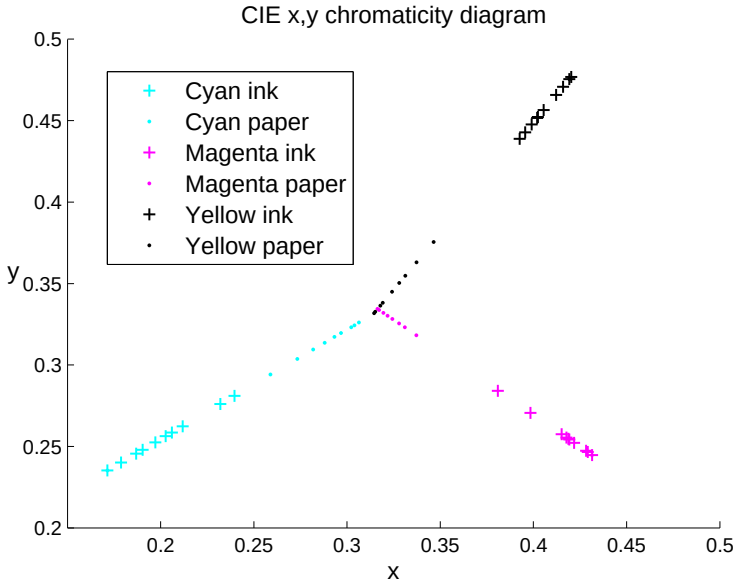

Figure 6. CIE chromaticity coordinates for the ink and for the paper between the dots, with varying dot area coverage. Cyan, magenta and yellow colorants, Paper A – AM.

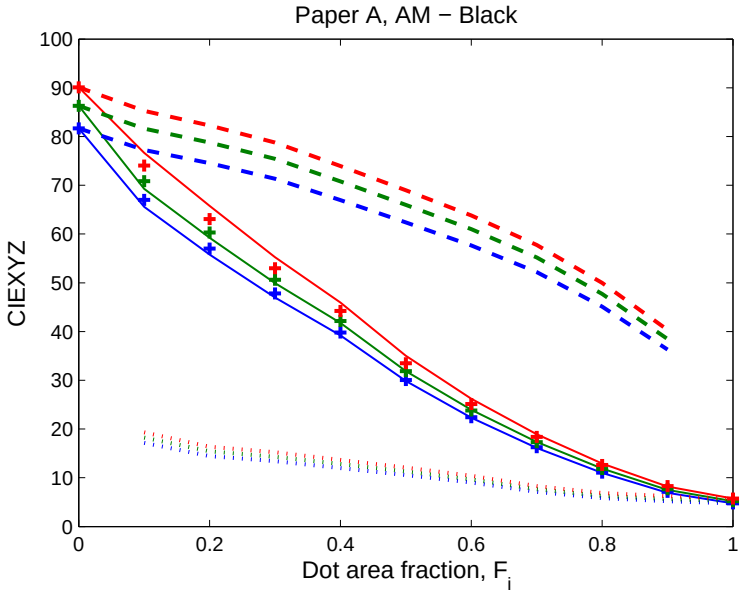

Figure 7. Measured CIEXYZ values (solid line), predicted (+), $XYZ_p(Fi)$ (dashed) and $XYZ_i(F_i)$ (dotted), for Paper A - AM.

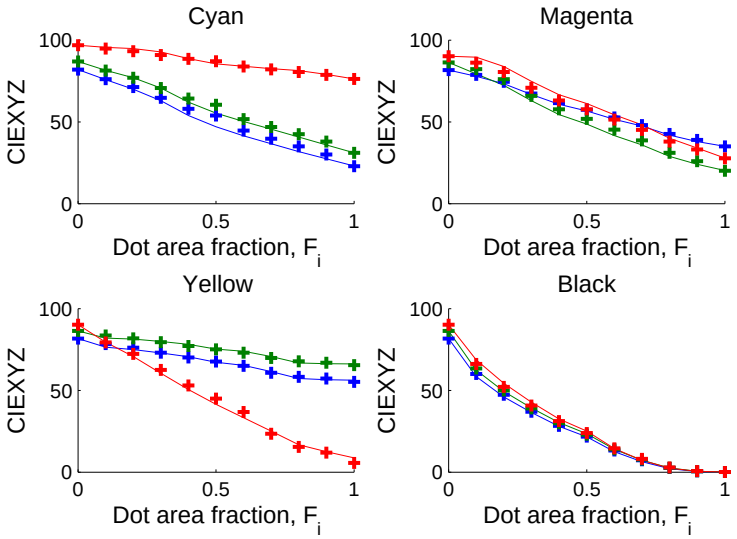

Figure 8. Measured (solid line) and predicted (+) mean CIEXYZ tristimulus values, for Paper A - FM.

Discussion and Continuation

This work focuses on micro-scale studies of halftone prints, especially how the reflectance of the printed dots and the paper between them, vary with respect to the dot area fraction. The reflectance values of the ink, $R_i(F_i)$, and paper, $R_p(F_i)$, are estimated for each area coverage, using histogram data for both grayscale and color halftones. The true dot area fraction, including the physical dot gain, is estimates using line scans in images, from transmission images of the halftones, and by using the midpoint of $R_i(F_i)$, and $R_p(F_i)$. The best results are obtained by using the line scan approach. Another option to compute the true dot area fraction could be to incorporate a previously proposed model, separating the optical dot gain from the physical dot gain (Yang, 2004).

For the color case, predicting tristimulus values, projections down to one-dimensional color distributions are used to overcome the difficulties when using the full 3D histograms to compute $XYZ_i(F_i)$, $XYZ_p(F_i)$ and F_i. A possible way to improve the proposed method of projection is to use principle component analysis, PCA. Defining the projection by the most significant eigenvector from the covariance matrix of all XYZ coordinates in the prints, will most likely provide a more robust method, compared to that using only the coordinates for the full tone and bare paper.

The validity of the extended Murray-Davies model, utilizing the varying reflectance $R_i(F_i)$ and $R_p(F_i)$ to account for the non linearity of optical dot gain, has been evaluated. It is shown that the model is valid, even for prints of considerably higher print resolution than those were previously tested. However, the FM halftones generally produce larger estimation errors, due to the difficulty in finding the proper peaks and threshold values from the histograms. A possible way to overcome this problem could be to incorporate an improved model for histogram analysis, developed specially for the case of noisy histograms from halftone images (Arney & Wong, 1998). The prediction errors of the model were found to be equivalent, or better, to the results of the Yule-Nielsen model, using optimal n-values. However, unlike the Yule-Nielsen model, the extended Murray-Davies model preserves the linear additivity of reflectance, thus providing a better physical description of the optical dot gain in halftone color prints. Since the Yule-Nielsen model assumes constant reflectance for the halftone dots and the paper between them, which has been proven wrong, it cannot be considered as a correct description of optical dot gain.

By using high-resolution colorimetric images of halftone color prints, it is possible to measure and characterize $R_i(F_i)$ and $R_p(F_i)$, i.e. how the color for the halftone dots and the paper between the dots varies with dot area fraction. The future studies should be to model the color shift phenomenon, especially with the focus to relate it to properties of the substrate, the print method and the halftone used. The combination of micro-scale imaging with colorimetric and

spectral accuracy, provide a powerful tool for the development of a deeper understanding of the complex phenomenon of optical dot gain. An understanding, crucial in the development of more sophisticated models of halftone color printing, which can benefit the print quality.

Literature Cited

Arney, J. S., Engeldrum, P.G. and Zeng, H.
1995a "An Expanded Murray-Davies Model of Tone Reproduction in Halftone Imaging", Journal of imaging science and technology, Vol.39, No. 6, pp 502-508.
1995b "A Modified Murray-Davies Model of Halftone Gray Scales", TAGA Proc., pp 353-363.

Arney, J. S. & Wong, Y-M.
1998 "Histogram Analysis of the Microstructure of Halftone Images", Proc. IS&T's 1998 Image Processing, Image Quality, Image Capture, Systems Conference, Portland.

Engeldrum, P. G.
1994 "The Color between the Dots", Journal of imaging science and technology, Vol.38, No. 6, pp 545-551.

Murray, A.
1936 "Monochrome reproduction in photoengraving", J Franklin Institute, 221, 721

Nyström, D.
2006." Colorimetric and Multispectral Image Acquisition". Licentiate Thesis No. 1289, Linköping University, Sweden.

Nyström, D.
2007 "Reconstructing Spectral and Colorimetric Data Using Trichromatic and Multi-channel Imaging", Proc. Ninth International Symposium on Multispectral Color Science and Application, Taipei, pp 45-52.

Nyström, D. & Kruse, B.
2005 "High resolution properties of color prints", Proc. CSIST/IS&T Beijing International Conference on Imaging, Beijing, pp 242-243.

Nyström, D. & Kruse, B.
2006 "Colorimetric Device Characterization for Accurate Color Image Acquisition", In Advances in Printing and Media Technology, Vol. 33, pp 349-360.

Pearson, M.
1980 "n Value for General Conditions", TAGA Proc., pp 415–425.

Wyble, D. R. & Berns, R. S.
2000 "A Critical Review of Spectral Models Applied to Binary Color Printing", Color research and application, volume 25, pp 4-19.

Yang, L.
2004 “A Unified Model of Optical and Physical Dot Gain in Print Color Reproduction”, Journal of imaging science and technology, Vol. 48, No. 4, pp 347-353

Yule J.A.C. & Nielsen W.J.
1951 “The Penetration of Light Into Paper and Its Effect on Halftone Reproductions”, TAGA Proc., 3, pp. 65–76.

Appendix: Experimental Setup

Image acquisition

An experimental image acquisition system is used, specially designed for acquiring micro-scale images of prints and substrates. The images are captured using a monochrome CCD camera, with a resolution of 1360 × 1024 pixels and 12 bit dynamic range. The CCD, specially designed for scientific imaging, is of grade 0, which means no defective pixels, and uses digital temperature compensation to reduce noise. It has previously been verified that the camera response is linear with respect to the intensity of the incident light (Nyström, 2006). The optics used is a macro system, designed for scientific applications, allowing for images of various magnifications, up to a maximal resolution of 1.2 μm/pixel.

The substrate is placed on a table which allows for controlled translations in two directions and for rotation around the optical axis. The illumination is provided using a tungsten halogen lamp through optical fibers, which offers an adjustable and well-controlled angle of incidence, as well as the possibility of using a backlight setup. Color images are captured sequentially, using filters mounted in a filter wheel in front of the light source. By using this color sequential method, there is no need for any interpolation or de-mosaicing scheme, as is the case in conventional digital cameras. Besides the ordinary RGB-filters, the filter wheel also contains a set of 7 interference filters, which allows for the acquisition of multi-channel images. The image acquisition system has previously been thoroughly calibrated and characterized. Models have been developed, allowing for the device dependent images to be converted into the (device independent) colorimetric representations CIEXYZ and CIELAB, and also to reconstruct spectral reflectance data (Nyström, 2006, Nyström & Kruse, 2006).

Micro-scale images

Grayscale and RGB images of various test prints have been captured using the 45˚/0˚ measurement geometry. The field of view was 2.7 × 2 mm, giving a resolution corresponding to 2μm/pixel. All images are first corrected for dark current and CCD gain. After calibration against a white reference, the pixel values for the grayscale images correspond to true reflectance values. The conversion to CIEXYZ color space was made by polynomial regression from

RGB images, using characterization functions individually derived for each print. The method has previously been verified to be sufficient, with a mean CIE 1976 color difference of 1.7 ΔE_{ab} and a maximum of 3.3 ΔE_{ab} (Nyström, 2007).

Printed samples

The printed samples used in the study consisted of offset prints on different paper grades, with both conventional halftoning (AM) and stochastic halftoning (FM). Test patches of primary colors and black were printed with nominal dot area coverage ranging from 0 to 100%, in 10% intervals. The details on the print samples are given in Tab. 3. Macroscopic measurements of the spectral reflectance values of the printed color patches were derived using a spectrophotometer, equipped with a UV filter. All colorimetric computations were made using the CIE standard illuminant D65.

Table 3. The printed halftone samples.

Paper A	Silk, 130 gr/m^2	1200 dpi	175 lpi
Paper B	Matt, 100 gr/m^2	800 dpi	150 lpi
Paper C	Matt, 100 gr/m^2	1200 dpi	150 lpi
Paper D	Gloss, 130 gr/m^2	1200 dpi	175 lpi
Paper E	Uncoated, 150 gr/m^2	800 dpi	150 lpi